Eur. Phys. J. A **13**, 21–26 (2002)

THE EUROPEAN PHYSICAL JOURNAL A

Properties unique in nuclei far from β stability line

I. Hamamoto

Division of Mathematical Physics, LTH, University of Lund, P.O. Box 118, S-22100 Lund, Sweden

Received: 1 May 2001

Abstract. Nucleons with very small binding energies present in nuclei far from the β stability line produce a unique shell structure, which leads to the disappearance of traditional magic numbers or to the creation of new magic numbers and new deformation regions. We study the shell structure in terms of the variation of two important ingredients, the kinetic energy and the spin-orbit splitting, as a function of the orbital angular momentum ℓ, when binding energies of neutrons decrease towards zero. It is also shown that for low-lying threshold strength, a negative sign is possible for the polarization charge coming from the coupling of one-particle to isoscalar shape oscillations.

PACS. 21.10.Pc Single-particle levels and strength functions – 21.60.Ev Collective models

1 Introduction

Nuclei far from β stability lines are expected to show some very interesting and exotic properties, due to a) the presence of nucleons with very small binding energy; b) the unconventional neutron/proton ratio for a given mass number; c) a large difference between the Fermi level of protons and that of neutrons. The presence of nucleons with binding energies less than 8–10 MeV, which is the separation energy typical of β stable nuclei, leads to unique shell structure, the long tail of the density and potential, low-lying threshold strength, larger width of giant resonances, and unique polarization due to the coupling to shape oscillations.

Available experimental information on ${}^{32}_{12}\mathrm{Mg}_{20}$, which is a singly closed-shell nucleus in the traditional terminology, indicates that the nucleus is deformed [1]. A new magic number $N = 16$ near the neutron drip line is recently suggested [2]. Furthermore, the dissipation of the magic number $N = 8$ is reported [3] from the measurement of low excitation energies of 2^+ and 1^- states and the observed large $B(E2)$ and $B(E1)$ values in the nucleus ${}^{12}_{4}\mathrm{Be}_{8}$.

First we examine one-particle shell structure for a given potential. In fig. 1 we plot one-particle energy eigenvalues for neutrons in Woods-Saxon potentials. The parameters of the potential in fig. 1a are those standard for β stable nuclei [4]. In fig. 1b the diffuseness parameter is doubled while all other parameters are the same as in fig. 1a. From fig. 1a it is seen that around $E_{n\ell} = -10$ MeV, which corresponds approximately to the Fermi level of β stable nuclei, the neutron numbers $N = 8$ and 20 are magic numbers as is well known in β stable nuclei. In contrast, for $E_{n\ell} = -2 \to 0$ MeV the $N = 8$ magic number disappears, while $N = 16$ becomes the new magic number. In the potential of fig. 1b we see that for $E_{n\ell} > -5$ MeV the magic numbers $N = 8$ and $N = 20$ disappear, while new magic numbers, $N = 16$ and 34, are observed. The above change of the magic numbers for $E_{n\ell} = -10 \to 0$ MeV originates from smaller values of $|\mathrm{d}E_{n\ell}/\mathrm{d}A|$ for smaller ℓ orbitals as $|E_{n\ell}|$ becomes smaller. Indeed, for finite square-well potentials one can analytically show that

$$\left.\frac{\mathrm{d}E_{n\ell}}{\mathrm{d}A}\right|_{E_{n\ell}=0} = \begin{cases} 0\,, & \text{for } \ell = 0\,, \\ \text{finite}\,, & \text{for } \ell > 0\,. \end{cases} \qquad (1)$$

The appearance of those new magic numbers should be seen from Hartree-Fock (HF) calculations, in which the one-body potential is obtained from the one-particle density in the presence of occupied neutrons with small binding energies. In fig. 2 an example of Skyrme HF calculations of ${}^{22}_{6}\mathrm{C}_{16}$ is shown. The possible presence of the neutron magic number $N = 16$ for very small binding energies is recognized, while the proton number $Z = 16$ obtained around -10 MeV does not correspond to any large energy gap in the one-particle level structure. In the same way the Skyrme HF calculation of ${}^{48}_{14}\mathrm{Si}_{34}$ indicates the possible presence of the neutron magic number $N = 34$ for very small binding energies of neutrons.

One must carefully examine fig. 1 in order to recognize any special variation of spin-orbit splittings for $|E_{n\ell}| \to 0$. This is because the mass number A is the variable in the x-axis of fig. 1, while the distance of one-particle energies decreases as A becomes larger, approximately proportional to $A^{-1/3}$. In figs. 1 and 2 of ref. [5] the one-particle level structure obtained from HF calculations is shown for given mass numbers $A = 120$ and 110, by varying the N/Z ratio from the proton to the neutron drip line. From those figures it is clearly seen that, for a given mass number, the neutron spin-orbit splitting of smaller ℓ orbitals

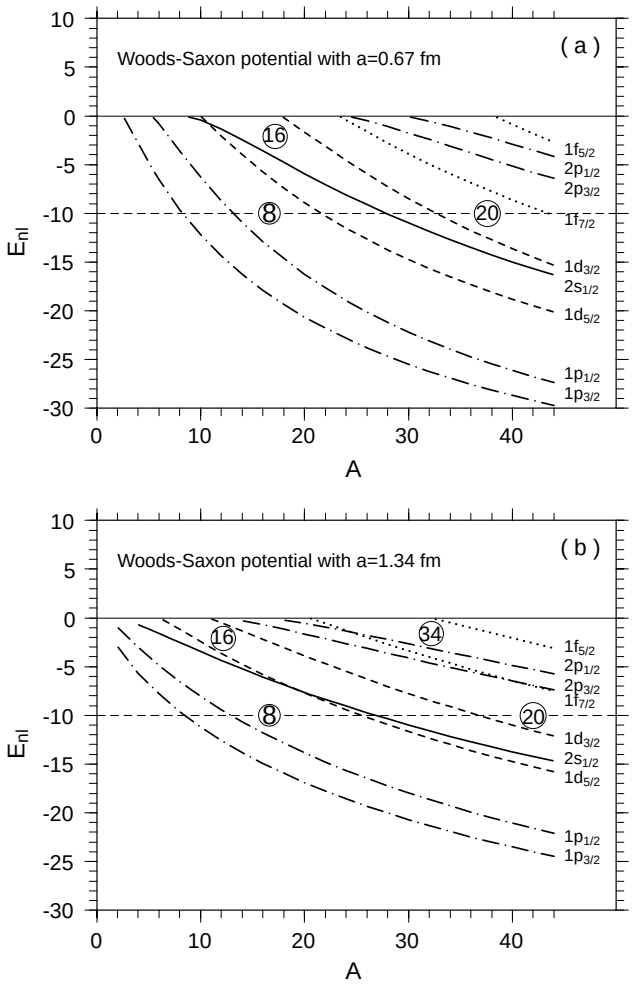

Fig. 1. Energies of neutron orbits: (a) for the Woods-Saxon potential with standard parameters [4]; (b) the same as (a) except for $a = 1.34$ fm.

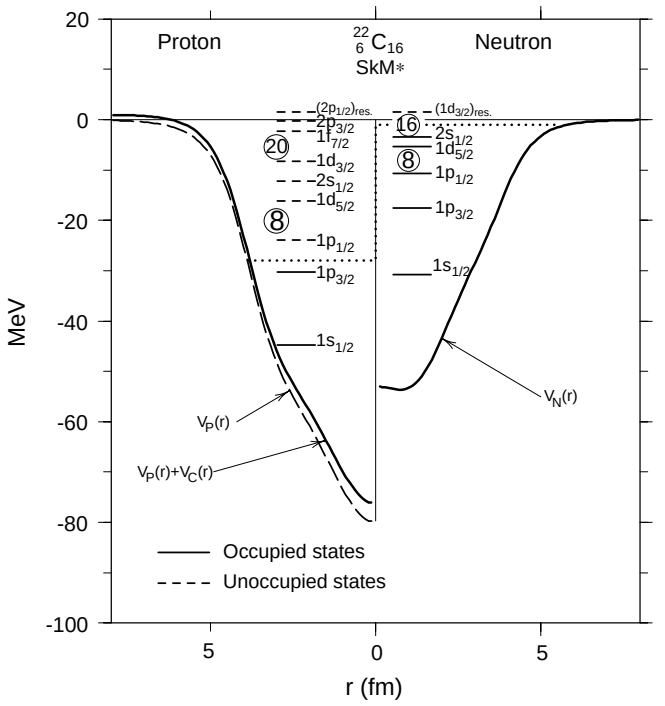

Fig. 2. HF potentials and one-particle levels of $^{22}_{6}C_{16}$. Neutrons on the r.h.s. and protons on the l.h.s. $V_{\rm N}(r)$ expresses the neutron nuclear potential, while $V_{\rm P}(r)$ and $V_{\rm C}(r)$ denote the proton nuclear potential and the Coulomb potential, respectively. The notation $(n\ell_j)_{\rm res}$ expresses the calculated one-particle resonant levels for the HF potential. Occupied levels are indicated by full lines, while unoccupied levels are denoted by broken lines.

becomes smaller in contrast to that of larger ℓ orbitals, as the neutron binding energies approach zero.

The one-particle operator, of which the expectation value gives kinetic energy in our prescription, is in fact the same as the particle-vibration coupling operator to shape oscillations. Thus, diagonal and non-diagonal matrix elements of the operator are proportional to the polarization charge. The polarization charge related to particles with very small binding energies may have a behavior unexpected from our common sense in the study of β stable nuclei. As an example we show that the polarization charge of $E2$ excitations of loosely bound particles to the continuum can be negative.

In sects. 2 and 3 the behavior of two important ingredients of the nuclear shell structure, kinetic energy and spin-orbit splitting, is studied [6] as a function of the orbital angular momentum ℓ and of binding energies, when neutron binding energies decrease towards zero. In sect. 4 we illustrate an unexpected negative sign of the polarization charge of $E2$ transitions coming from the coupling of particles near threshold to shape oscillations. In sect. 5 conclusions are given.

2 One-particle kinetic energy

One-particle eigenenergy ϵ_ν is the sum of the positive kinetic and negative potential energy:

$$\epsilon_\nu \;=\; \langle\nu|T|\nu\rangle + \langle\nu|V(r)|\nu\rangle\,. \qquad (2)$$

For bound states, $\epsilon_\nu < 0$, the absolute magnitude of the potential energy $\langle V\rangle$ which is negative, is larger than the kinetic energy $\langle T\rangle$. In the case of larger ℓ orbitals $|\langle V\rangle|$ becomes smaller while $\langle T\rangle$ gets larger, as $|\epsilon_\nu| \to 0$. In contrast, for smaller ℓ orbitals $\langle T\rangle$ does not become larger as $|\epsilon_\nu| \to 0$, since one-particle wave functions can extend beyond the potential due to lower centrifugal barriers. Consequently, the second derivative of one-particle wave functions by the radial coordinate (namely the kinetic energy) may decrease. As a result of it, $|\epsilon_\nu|$ of smaller ℓ orbitals approaches zero very slowly. In the following we demonstrate this situation.

The one-body potential in nuclei is written as

$$V(r) \;=\; U(r) \,+\, V_{\ell s}(r) \,+\, V_{\rm C}(r)\,. \qquad (3)$$

The expectation value of the kinetic energy is calculated for simple potentials $U(r)$: infinite square-well potential, finite square-well potential and Woods-Saxon potential. Using eigenfunctions with quantum numbers $(n\ell)$ in the

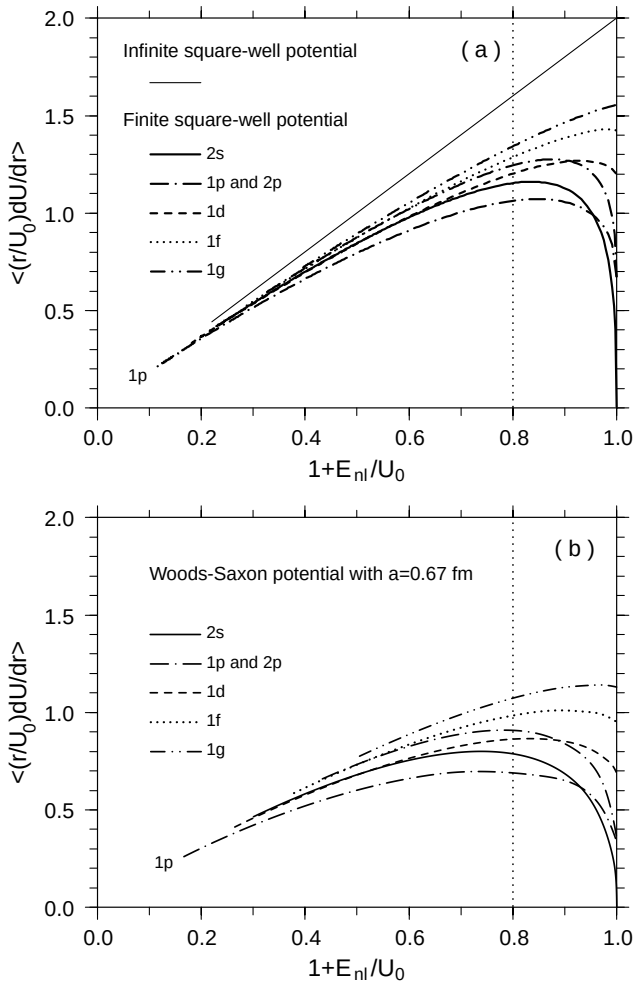

Fig. 3. Expectation values of (6), which are proportional to the kinetic energy of the respective one-particle orbitals, as a function of $(1+(E_{n\ell}/U_0))$. For $U_0 = 50$ MeV, $(1+(E_{n\ell}/U_0)) = 0.8$ and 1.0 mean $E_{n\ell} = -10$ and 0 MeV, respectively. Figures are taken from ref. [6]. (a) For the square-well potential with $U_0 = 50$ MeV. For the infinite square-well potential, the thin straight line is common for all orbitals with various (n, ℓ) values. (b) For the Woods-Saxon potential with standard parameters.

absence of the Coulomb and spin-orbit potential

$$(T + U(r))\,|n\ell\rangle \;=\; E_{n\ell}\,|n\ell\rangle\,, \tag{4}$$

the expectation value of the kinetic energy can be written as

$$\langle n\ell\,|T|n\ell\,\rangle \;=\; \frac{1}{2}\left\langle n\ell\left|\, r\,\frac{\mathrm{d}U(r)}{\mathrm{d}r}\right|\, n\ell\right\rangle\,, \tag{5}$$

due to the virial theorem. The r.h.s. expression of (5) is especially useful when the kinetic energy is later compared with the spin-orbit splitting.

We write the kinetic energy in the form of (5), which is expressed in terms of the radial derivative of the one-body potential. It is interesting to note that diagonal and non-diagonal matrix elements of the same operator, $r\frac{\mathrm{d}U(r)}{\mathrm{d}r}$, express the coupling to shape oscillations and thus are proportional to the polarization charge.

In fig. 3 the expectation values of the operator

$$\frac{r}{U_0}\,\frac{\mathrm{d}U(r)}{\mathrm{d}r} \tag{6}$$

for neutrons are shown for an infinite square-well potential, a finite square-well potential with depth $U_0 =$ 50 MeV, and the Woods-Saxon potential with standard parameters [4] with $U_0 = 50$ MeV, $N = Z$ and $v_{\ell s} = 0$, as a function of $(1 + (E_{n\ell}/U_0))$. For $U_0 = 50$ MeV $(1+(E_{n\ell}/U_0)) = 0.8$ and 1.0 mean $E_{n\ell} = -10$ and 0 MeV, respectively.

Since our potential $U(r)$ has a finite range, the contribution to the one-particle expectation value of (6) comes from the part of one-particle wave functions inside the range. In the infinite square-well potential ($U_0 \to \infty$), the kinetic energy is equal to $U_0 + E_{n\ell}$ and, thus, the expectation values of (6) multiplied by U_0 are given by $2(U_0+E_{n\ell})$ for all orbitals independent of (n, ℓ) values. We note that in this potential, one-particle wave functions cannot extend to the outside of the potential and, thus, the reduction in the increasing rate of the kinetic energy never occurs as $(1 + (E_{n\ell}/U_0))$ increases. For finite square-well potentials the probability for one particle to stay inside the potential in the limit of zero binding energy can be analytically calculated and is equal to 0, 0.33 and 0.60 for $\ell = 0$, 1 and 2, respectively [7]. The extension of one-particle wave functions with smaller ℓ values to the outside of the potential is the origin of the decrease of the kinetic energy as well as of the spin-orbit splitting, when the binding energies become smaller.

The vertical dotted line in fig. 3 at $(1 + (E_{n\ell}/U_0)) =$ 0.8, namely $E_{n\ell} = -10$ MeV for $U_0 = 50$ MeV, indicates the approximate Fermi level of β stable nuclei. When the eigenvalue $E_{n\ell} \to 0$ exists for the potential with a finite range, the expectation value of (6) for $(n, \ell = 0)$ orbitals in the finite-well potential, approaches zero, since, due to the absence of centrifugal barrier, the $\ell = 0$ neutron wave functions can extend up to infinity. For the finite square-well potential the expectation value of (6) at $E_{n\ell} = 0$ is independent of n and is equal to 2/3, 6/5 and 10/7, for the $\ell = 1$, 2 and 3 orbitals, respectively [8]. The expectation value for Woods-Saxon potentials depends on the radial node n.

From fig. 3 it is seen that a considerable deviation from the straight line occurs first at smaller values of $|E_{n\ell}|$ for a less diffuse potential and for larger ℓ orbitals. As seen in fig. 3a, for the square-well potential the kinetic energy starts to decrease first at very small binding energies, even for $\ell = 0$ orbitals.

3 Spin-orbit splitting

The spin-orbit potential in (3) is written as

$$V_{\ell s}(r) = c\,(\vec{\ell}\cdot\mathbf{s})\,\frac{1}{r}\,\frac{\mathrm{d}U(r)}{\mathrm{d}r}\,, \tag{7}$$

where c is a constant which is usually determined in a phenomenological way. Thus, using eigenfunctions $|n\ell\rangle$ in

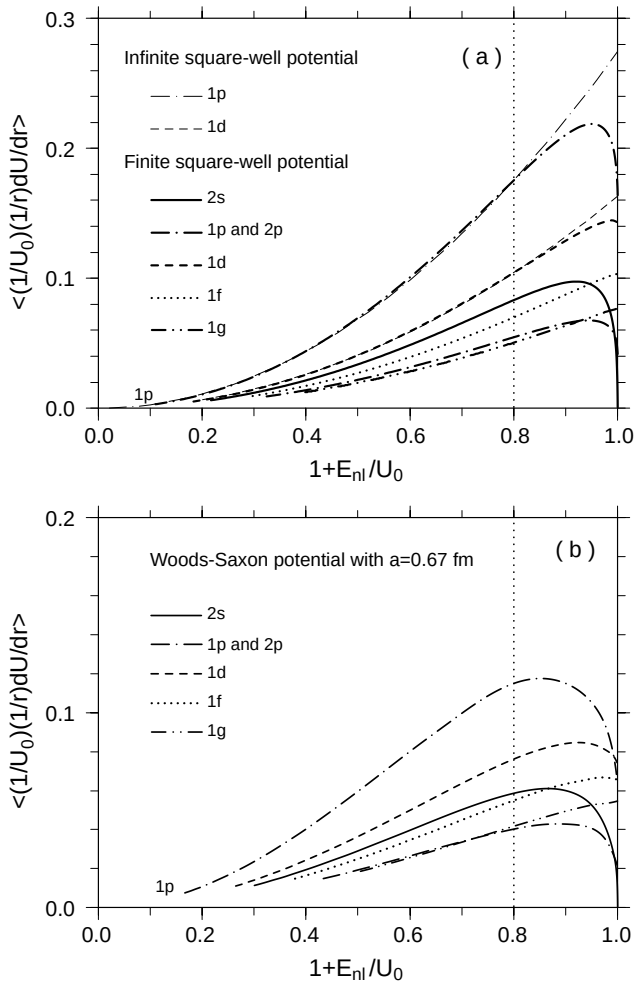

Fig. 4. Expectation values of the operator (9), which are proportional to the spin-orbit splitting of the ℓ orbital when multiplied by $(2\ell+1)$, as a function of $(1+(E_{n\ell}/U_0))$. Figures are taken from ref. [6]. (a) For square-well potential with $U_0 = 50$ MeV. The thin curves express those corresponding to infinite square-well potential, which are normalized so as to coincide at $(1+(E_{n\ell}/U_0)) = 0.8$ with those of the same quantum numbers $(n\ell)$ for the finite square-well potential. (b) For the Woods-Saxon potential with standard parameters.

eq. (4), namely treating $V_{\ell s}(r)$ by perturbation, one obtains

$$\text{spin-orbit splitting} \propto (2\ell+1)\left\langle n\ell\left|\frac{1}{r}\frac{\mathrm{d}U(r)}{\mathrm{d}r}\right|n\ell\right\rangle . \quad (8)$$

In fig. 4 the expectation values of the operator

$$\frac{1}{r\,U_0}\frac{\mathrm{d}U(r)}{\mathrm{d}r} \quad (9)$$

for neutrons are shown for the same simple potentials as those used in sect. 2. The thin curves in fig. 4a are estimated for the infinite square-well potential, normalizing the curve at $(1+(E_{n\ell}/U_0)) = 0.8$ so that it coincides with the corresponding curve for the finite square-well potential. See ref. [6] for details. Our purpose is to compare the result of finite potentials with that of the infinite potential, in order to see the effect of the presence of a surface. It is seen that only in the region of $(1+(E_{n\ell}/U_0)) > 0.8$ the curve for the finite square-well potential differs appreciably from that for the infinite square-well potential. For potentials with a diffuse surface the expectation values of (9) start to decrease at smaller values of $(1+(E_{n\ell}/U_0))$, as seen from the comparison between figs. 4a and 4b. The decrease is more appreciable for orbitals with smaller ℓ values.

The plotted quantity in fig. 4 times $(2\ell+1)$ is proportional to the spin-orbit splitting. For a given $E_{n\ell}$ value the spin-orbit splitting for the $1p$ orbitals is much larger than that for the $2p$ orbital, since the former belongs to lighter nuclei. The variation of spin-orbit splitting of orbitals with a given ℓ for $E_{n\ell} = -10 \to 0$ MeV depends moderately on the radial node n.

The extension of one-particle wave functions with smaller ℓ values to the outside of the potential is the origin of the decrease of spin-orbit splitting when the binding energies become smaller, as in the case of the kinetic energy described in sect. 2. Due to the different r-dependence in (6) and (9), the effect of the diffuse surface on the kinetic energy starts to appear already at deeper bound orbitals compared with the spin-orbit splitting.

4 Coupling of particles near threshold to shape oscillations

The λ-pole polarization charge coming from the coupling to λ-pole isoscalar (IS) shape oscillations is written as [9]

$$(e_{\mathrm{pol}})_{\lambda,\,\tau\approx 0} = \frac{\langle j_2|R\,\frac{\mathrm{d}V(r)}{\mathrm{d}r}|j_1\rangle}{\langle j_2|r^\lambda|j_1\rangle}\,\frac{3}{4\pi}\,\frac{ZeR^\lambda}{C_\lambda}\,\frac{(\hbar\omega_\lambda)^2}{(\hbar\omega_\lambda)^2-(E_2-E_1)^2}\,, \quad (10)$$

where the nuclear radius is expressed by R and the form factor of shape oscillations by $R\frac{\mathrm{d}V}{\mathrm{d}r}$, the matrix elements of which are almost the same as those of $r\frac{\mathrm{d}V}{\mathrm{d}r}$. In fact, the form factor $R\frac{\mathrm{d}V}{\mathrm{d}r}$ or $r\frac{\mathrm{d}V}{\mathrm{d}r}$ may be used also for isovector (IV) modes in an approximation. The last factor in eq. (10) is close to unity, when either static polarization ($E_2 = E_1$) or coupling to giant resonances ($\hbar\omega_\lambda \gg |E_2 - E_1|$) is considered. Then, the sign of the polarization charge in (10) is given by that of the ratio

$$\frac{\langle j_2|R\,\frac{\mathrm{d}V(r)}{\mathrm{d}r}|j_1\rangle}{\langle j_2|r^\lambda|j_1\rangle}\,. \quad (11)$$

The form factor $R\frac{\mathrm{d}V}{\mathrm{d}r}$ is surface peaked for any reasonable nuclear potential, and the major contribution to $\langle r^\lambda\rangle$ comes also from the surface region if relevant particle orbitals j_1 and j_2 are sufficiently well bound. Thus, for the harmonic-oscillator model or for well-bound particles, which have been traditionally studied in β stable nuclei, the sign of the ratio (11) is always positive. This positive sign leads to the result $(e_{\mathrm{pol}})_{\lambda,\,\tau\approx 0} > 0$, namely

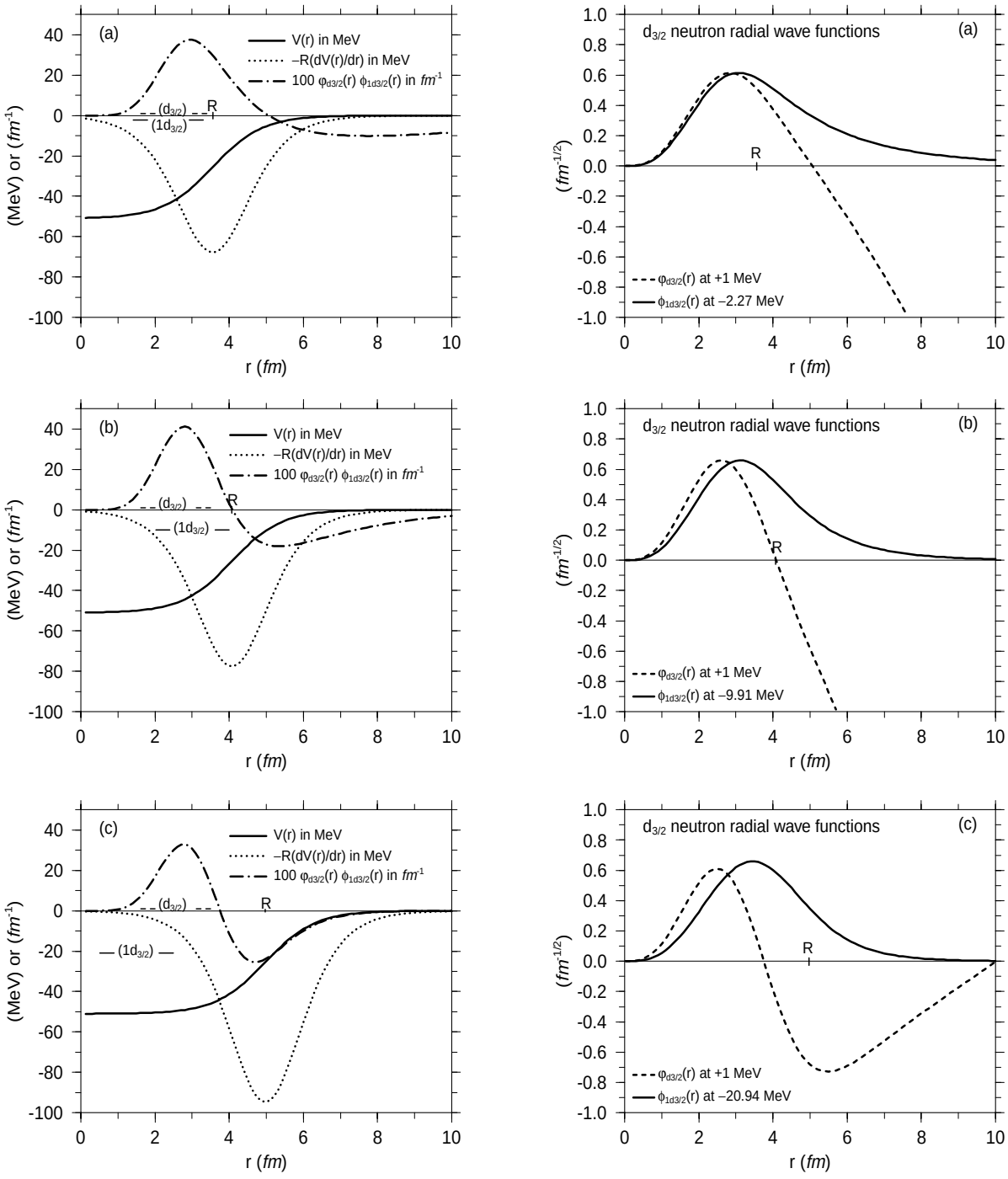

Fig. 5. r.h.s.: $d_{3/2}$ neutron radial wave functions. For (a)-(c) dashed curves show $\varphi_{d3/2}(r)$ calculated at $E = +1$ MeV. Solid curves denote $\phi_{1d3/2}(r)$ calculated at $E = -2.27$, -9.91 and -20.94 MeV for (a), (b) and (c), respectively, which are eigenenergies of the respective Woods-Saxon potentials shown by solid curves on the l.h.s. figures. The radius of the respective potentials is indicated by R. l.h.s.: Woods-Saxon potentials $V(r)$, $-R(\mathrm{d}V(r)/\mathrm{d}r)$ and the product $\varphi_{d3/2}(r)\phi_{1d3/2}(r)$. Energies of the $(d_{3/2})$ and $(1d_{3/2})$ states are denoted in the respective figures.

the fact [9] that the attractive coupling to IS shape oscillations produces an increase of the low-lying transition strength which is proportional to $|\langle j_2|r^\lambda|j_1\rangle|^2$.

Using the analytic expressions with the square-well potential, in ref. [8], we have examined the polarization charge of particles with very small binding energies. It is shown that the quadrupole polarization charge coming from the coupling of particles with ℓ to the IS quadrupole shape oscillations becomes

$$(e_{\rm pol})_{\lambda=2,\,\tau\approx 0} \to 0\,, \quad \text{for } \ell = 0 \text{ and } 1 \tag{12}$$

and

$$(e_{\rm pol})_{\lambda=2,\,\tau\approx 0} > 0\,, \quad \text{for } \ell \geq 2 \tag{13}$$

in the limit of zero binding energies of the particles.

In the excitation of a bound particle with quantum numbers $(n_h\ell_h)$ to a continuum particle state with energy E_c and orbital angular momentum ℓ_c, the analytic expression of the ratio

$$\frac{\langle \ell_c|R\,\frac{{\rm d}V(r)}{{\rm d}r}|n_h\ell_h\rangle}{\langle \ell_c|r^2|n_h\ell_h\rangle}\,, \tag{14}$$

for the square-well potential is given in ref. [8]. We have concluded: a) For small values of ph excitation energies (namely, both the particle energy in the continuum and the separation energy of the $(n_h\ell_h)$ bound particle are small), the sign of the ratio (14) can be negative when the separation energy of the least-bound one-particle orbital with ℓ_c, which is an eigenstate of the potential, is small. For example, the sign is always negative for very low-energy ph excitations with $\ell_h = \ell_c$. b) When the separation energy of the least-bound one-particle with ℓ_c becomes larger than a certain value, which is about -10 MeV for the Woods-Saxon potential with standard parameters, the sign becomes positive even for small values of particle energy in the continuum. Then, the sign of the ratio (14) is positive even for small values of ph excitation energies.

Taking the excitation of one particle in the $1d_{3/2}$ orbital, which is the eigenstate of respective Woods-Saxon potentials, to the continuum $d_{3/2}$ orbital at $+1$ MeV, in fig. 5 we illustrate the dependence of the sign of the factor (14) on the eigenenergy of the $1d_{3/2}$ orbital; (a) -2.27 MeV, (b) -9.91 MeV and (c) -20.94 MeV. Parameters of the Woods-Saxon potential are those standard ones [4]. The only parameter which is different in (a)-(c) is the radius, R, (or mass number) so that the $1d_{3/2}$ orbital is the eigenmode with respective binding energies. On the r.h.s. radial wave functions, $\varphi_{d3/2}(r)$ and $\phi_{1d3/2}(r)$, are shown, while on the l.h.s. the product $\varphi_{d3/2}(r)\phi_{1d3/2}(r)$ is shown together with the respective Woods-Saxon potentials, $V(r)$, and $-R({\rm d}V(r)/{\rm d}r)$. We note that the sign of the r^2 matrix element is always the same as that of $\varphi_{d3/2}(r)\phi_{1d3/2}(r)$ outside the nucleus. Thus, in the case of (a) the factor (14) is negative, while in (c) it is positive. In the case of (b) the matrix element of $R({\rm d}V(r)/{\rm d}r)$ almost vanishes. It is seen that in β stable nuclei, in which the separation energy of neutrons is about 8–10 MeV, the sign of the factor (14) is always positive. In contrast, for the low-lying threshold strength in nuclei towards the neutron drip line the sign can be negative [8], as seen from the example in fig. 5(a).

5 Conclusions

When one-particle energies vary as $E_{n\ell} = -10 \to 0$ MeV, we have shown that a) both the kinetic energy and spin-orbit splitting decrease more strongly for small ℓ orbitals; b) the decrease is stronger for more diffuse potentials; c) the kinetic energy is more sensitive to the diffuse surface of potentials than the spin-orbit splitting. The variation of both the kinetic energy and the spin-orbit splitting is certainly playing an important role in the observation that around the neutron drip line the traditional magic numbers $N = 8$ and 20 disappear while the new magic number $N = 16$ appears. In shell model calculations of drip line nuclei one has to take properly into account those basic elements in the change of shell structure.

It is concluded that the IS (IV) strength in the energy region just above the low-lying threshold strength, which is created by exciting particles with small binding energies to the continuum in nuclei far from β stability lines, can be reduced (increased) by the attractive (repulsive) coupling to IS (IV) shape oscillations. This is in contrast to the well-known fact that in β stable nuclei low-lying IS (IV) particle-hole strengths are increased (reduced) by the attractive (repulsive) IS (IV) coupling.

I would like to express my sincere thanks to professor M. Ishihara for his inspiring discussions and continuous encouragements, which I have received since our student days.

References

1. D. Guillemaud-Mueller *et al.*, Nucl. Phys. A **426**, 37 (1984); T. Motobayashi *et al.*, Phys. Lett. B **346**, 9 (1995).
2. A. Ozawa, T. Kobayashi, T. Suzuki, K. Yoshida, I. Tanihata, Phys. Rev. Lett. **84**, 5493 (2000).
3. H. Iwasaki *et al.*, Phys. Lett. B **481**, 7 (2000); H. Iwasaki, this issue p. 55.
4. A. Bohr, B.R. Mottelson, *Nuclear Structure*, Vol. **I** (Benjamin, Reading MA, 1969) p. 239.
5. I. Hamamoto, H. Sagawa, X.Z. Zhang, Phys. Rev. C **53**, 765 (1996).
6. I. Hamamoto, S.V. Lukyanov, X.Z. Zhang, to be publiashed in Nucl. Phys. A.
7. K. Riisager, A.S. Jensen, P. Moller, Nucl. Phys. A **548**, 393 (1992).
8. I. Hamamoto, X.Z. Zhang, Phys. Rev. C **58**, 3388 (1998).
9. A. Bohr, B.R. Mottelson, *Nuclear Structure*, Vol. **II** (Benjamin, Reading MA, 1975).